

Evaluation of ion collection area in Faraday probes

Daniel L. Brown¹ and Alec D. Gallimore²

¹*Spacecraft Branch, Propulsion Directorate, Air Force Research Laboratory, Edwards AFB, California 93524, USA*

²*Department of Aerospace Engineering, Plasmadynamics and Electric Propulsion Laboratory, The University of Michigan, Ann Arbor, Michigan 48109, USA*

(Received 15 March 2010; accepted 18 May 2010; published online 25 June 2010)

A Faraday probe with three concentric rings was designed and fabricated to assess the effect of gap width and collector diameter in a systematic study of the diagnostic ion collection area. The nested Faraday probe consisted of two concentric collector rings and an outer guard ring, which enabled simultaneous current density measurements on the inner and outer collectors. Two versions of the outer collector were fabricated to create gaps of 0.5 and 1.5 mm between the rings. Distribution of current density in the plume of a low-power Hall thruster ion source was measured in azimuthal sweeps at constant radius from 8 to 20 thruster diameters downstream of the exit plane with variation in facility background pressure. A new analytical technique is proposed to account for ions collected in the gap between the Faraday probe collector and guard ring. This method is shown to exhibit excellent agreement between all nested Faraday probe configurations, and to reduce the magnitude of integrated ion beam current to levels consistent with Hall thruster performance analyses. The technique is further studied by varying the guard ring bias potential with a fixed collector bias potential, thereby controlling ion collection in the gap. Results are in agreement with predictions based on the proposed analytical technique. The method is applied to a past study comparing the measured ion current density profiles of two Faraday probe designs. These findings provide new insight into the nature of ion collection in Faraday probe diagnostics, and lead to improved accuracy with a significant reduction in measurement uncertainty. © 2010 American Institute of Physics. [doi:10.1063/1.3449541]

I. INTRODUCTION

Accurate measurement of ion current density in the plume of electric propulsion systems is required to study beam divergence and to quantify ion beam current. Faraday probe current density measurements are typically used for qualitative evaluation of the plume profile as opposed to quantitative assessment since calculations of total ion beam current are often greater than the thruster discharge current. Numerous studies have attributed this discrepancy to facility effects,¹⁻³ and many have aimed at mitigating these ground-based effects through extensive study of probe design modifications, experimental methods, and analytical techniques.⁴⁻⁷

Ion collection attributes of Faraday probe electrodes have not been thoroughly evaluated for in-space plasmas since the uncertainty associated with design geometry is generally assumed to be insignificant compared to the uncertainty associated with ground facility effects. The plasma generated in electric propulsion devices are significantly lower in density and/or energy than past investigations of Faraday cups that evaluated laser-produced plasmas,⁸ dense plasma focus discharges,^{9,10} or energetic electron beams.¹¹ Faraday cup behavior in these investigations was shown to be influenced by secondary electron emission (SEE), space-charge effects, and ambient pressure.

Although there are numerous Faraday cup configurations of varying complexity, a simple planar Faraday probe design

operates with equal bias potential applied to an ion collector and an outer guard ring, thereby creating a flat uniform sheath above the collector electrode to repel plasma electrons. According to conventional design criterion, the gap between collector and guard ring should be less than 10 Debye lengths to maintain a flat uniform sheath above the collector and minimize fringing fields around the edge.³ A past comparison of two planar Faraday probe designs surmised the differences in measured current density of a Hall thruster plume were due to probe geometry and dissimilar SEE properties of the probe collector materials.⁷ Although SEE characteristics have been evaluated for different collector materials,¹² the effects of probe geometry have not been methodically investigated.

The aim of this investigation is to increase accuracy and systematically evaluate the measurement uncertainty of Faraday probe current density associated with collector geometry. A nested Faraday probe was designed to examine the gap width and collector diameter. Facility effects on the collected ion current are quantified and isolated from differences due to probe design by adjusting facility background pressure and measurement distance from the thruster exit plane. Isolation of facility effects enabled a direct evaluation of the diagnostic ion collection properties as a function of geometric design with four configurations of the nested Faraday probe. This paper develops a hypothesis to explain the nature of ion collection in Faraday probes and proposes analytical techniques to assess the ion collection area. The

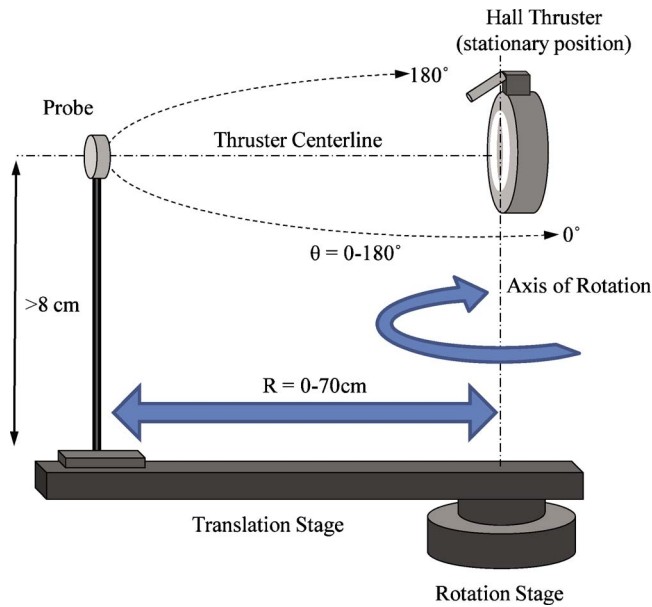


FIG. 1. (Color online) Diagnostic positioning system in chamber 1 with R, θ -coordinate axis control.

proposed analytical techniques are studied with variations in the guard ring bias potential, and are further examined by applying the methods to a past investigation comparing nude Faraday probe designs.^{3,7}

II. EXPERIMENTAL APPARATUS

A. Vacuum facility and Hall thruster ion source

The investigation was conducted at the Spacecraft Branch of the Air Force Research Laboratory (AFRL) in chamber 1, a stainless steel, cylindrical vacuum chamber 2.3 m in diameter and 4 m in length. An Edwards DryStar GV160 mechanical booster pump reached rough vacuum and lighter gases were removed with a Varian TV55 turbomolecular pump. Two CVi TorrMaster cryotubs circulated liquid nitrogen to cool four cryopanel, and achieved a maximum xenon pumping speed of 50 000 l/s. An MKS Instruments cold cathode ionization gauge was located on the chamber ceiling above the thruster centerline, and background pressure was increased by injecting xenon propellant through an auxiliary flow line located less than 1 m downstream of the thruster exit plane.

The ion source for these experiments was a low-power laboratory Hall thruster. Prior to Faraday probe data collection, the thruster was fired for over 1 h after initial startup. Thruster telemetry was monitored during Faraday probe sweeps, and exhibited negligible deviation from steady-state operation.

The Faraday probe (R, θ)-positioning system consisted of a translation stage for control of measurement radius and a rotation stage, which was centered beneath the exit plane on thruster centerline. In Fig. 1, one end of the translation stage is shown mounted on top of the rotation stage, enabling current density scans from 0° to 180° at constant radius up to 70 cm from the axis of rotation at the exit plane. A National

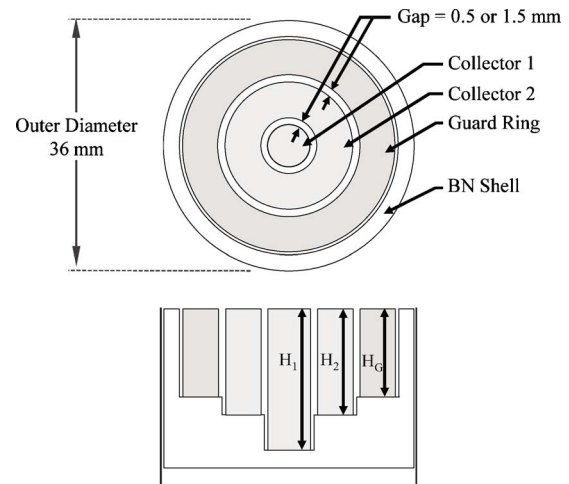


FIG. 2. (Color online) Top view and cross-sectional diagrams of the AFRL nested Faraday probe.

Instruments MID-7604/7602 Power Drive interfaced with the rotation and translation stages, and data acquisition was controlled through LABVIEW.

B. Nested Faraday probe

The nested Faraday probe consisted of two concentric collector rings and an outer guard ring, which enabled simultaneous current density measurements on the inner and outer collectors. The inner collector is designated collector 1 and the outer collector is designated collector 2. Two versions of collector 2 were fabricated to create gaps of either 0.5 or 1.5 mm between the rings. For either version of collector 2, the gap between collector 1 and collector 2 is always the same as the gap between collector 2 and the guard ring. The collectors and guard ring are seated within a boron nitride shell and are different heights to form a highly concentric probe with uniform gap width, as illustrated in the diagram in Fig. 2. These heights are labeled H_1 , H_2 , and H_G for collector 1, collector 2, and the guard ring, respectively. Probe dimensions are listed in Table I.

Past experimental measurements of the Hall thruster ion source beam indicated that the Debye length ranged from ~ 0.05 to ~ 1 mm throughout the plume from 8 to 20 channel centerline diameters downstream (CCDD) from the exit plane.¹³ Thus, the 0.5 mm gap configuration is expected to be less than or equal to 10 Debye lengths for all locations studied with the nested Faraday probe. The 1.5 mm gap configuration is greater than 10 Debye lengths, and is oversized to highlight effects of a gap width greater than the 10 Debye length design criteria.

Four ion collection geometries are studied using the nested Faraday probe. These configurations are shown in Fig. 3 and referred to as follows.

- (1) Configuration 1: current to collector 1 with a 0.5 mm gap.
- (2) Configuration 2: combined current to collectors 1 and 2 with a 0.5 mm gap.
- (3) Configuration 3: current to collector 1 with a 1.5 mm gap.

TABLE I. Nested Faraday probe dimensions.

	Collector 1	Collector 2		Guard ring
		0.5 mm gap	1.5 mm gap	
Inner diameter (mm)	...	7.06	9.16	20.27
Outer diameter (mm)	6.11	18.91	17.06	29.93
Height (mm)	15.58	13.75	13.76	10.22
Collector 1–2 gap (mm)	...	0.48	1.53	...
Collector 2–guard ring gap (mm)	...	0.68	1.61	...

- (4) Configuration 4: combined current to collectors 1 and 2 with a 1.5 mm gap.

For either the 0.5 or 1.5 mm gap configuration, the current collected by collector 1 is compared to the combined current on collector 1 and collector 2 (termed collector 1+2). Adding the collected current isolated effects caused by the inner gap to collector 1 from effects caused by the outer gap to collector 1+2. If the collected current were not added, collector 2 may be influenced by effects between the inner gap (collector 1 with collector 2) and the outer gap (collector 2 with the guard ring). This analysis allowed comparison of simultaneous measurements to different collection cross sections with the same gap width.

The nested Faraday probe collectors were machined from arc-cast low-carbon grade-365 molybdenum, and the guard ring is grade-360 molybdenum. Differences in SEE between the collectors and guard ring due to electrode material and surface roughness should be negligible. Collection surfaces were machined to a 32-microinch AA finish. A 20 cm long stainless steel tube houses the boron nitride shell and probe leads. This housing extends to the probe face and is grounded to create known boundary conditions for numerical simulations. Trials with the stainless steel housing allowed to float caused no change in collected current. All

subsequent measurements were taken with the housing connected to chamber ground.

Collected currents on both collectors and the guard ring were measured with an Agilent 34970A Data Acquisition/Switch Unit. An Agilent E3631A Triple Output dc power supply was used to bias the collectors and guard ring. The nested Faraday probe operation was characterized with variations in probe bias potential over a range of angular positions and downstream distances at several facility background pressures. A bias potential of -20 V with respect to facility ground was beyond the ion current saturation limit in all cases, and was used for all Faraday probe measurements unless otherwise noted in Sec. IV B.

III. RESULTS

Current density in the plume of a low-power Hall thruster was measured in angular sweeps from $\theta=0^\circ$ to 180° at distances of 8, 12, 16, and 20 CCDD from the ion source. Far-field measurements were taken for a hemispherical, axisymmetric coordinate system. Angular measurements were taken in 2° increments.

Normalized ion current density profiles of the four collector configurations are shown at 8, 12, 16, and 20 CCDD in Fig. 4. All profiles are normalized to the peak current density of configuration 1 at 8 CCDD. The current density measured by collector 1 was consistently larger than collector 1+2, and the 1.5 mm gap configurations measured a larger current density than the 0.5 mm gap configurations. These differences were uniform over the entire profile. Configuration 3 measured the maximum current density at a given scan radius, followed by configurations 1, 4, and 2. Although the 1.5 mm gap is larger than 10 Debye lengths and may be expected to cause discrepancies between configurations 3 and 4, the 0.5 mm gap configurations were expected to measure equivalent current density profiles. However, comparison of the 0.5 mm gap configurations reveals that the current density of configuration 1 is approximately 10% larger than the current density of configuration 2.

It is noted that current density measurements using the 0.5 mm gap were taken during separate thruster firings from the 1.5 mm gap configuration. However, differences in operation of the ion source were minimal, and would not explain the large discrepancies of configuration 1 compared to configuration 2. Configuration 2 was the only probe configuration to result in an integrated ion beam current less than the Hall thruster discharge current.

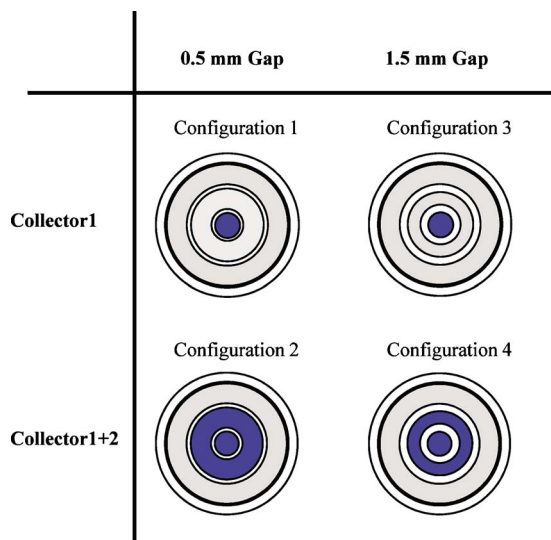


FIG. 3. (Color online) Top view of the four collection area configurations of the nested Faraday probe. Dark shaded regions indicate the current collecting surfaces orthogonal to the beam. The gap between collector 1 and collector 2 is approximately equal to the gap between collector 2 and the guard ring.

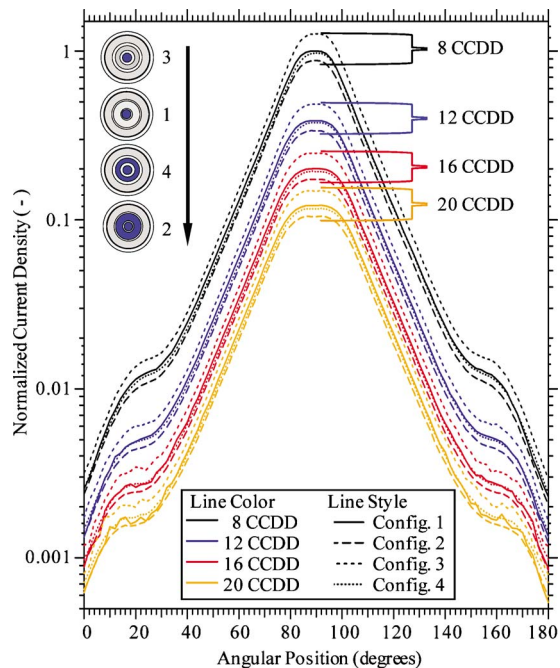


FIG. 4. (Color online) Normalized current density profiles from collector 1 and collector 1+2 for the 0.5 and 1.5 mm gap configurations measured at 8, 12, 16, and 20 CCDD with a facility background pressure of 3.1×10^{-6} torr.

In this investigation of probe geometric effects on collected current, it is assumed that the ion current density is constant across the probe surface. Therefore at a given location in the plume, the nested Faraday probe measurements should yield equivalent ion current density. For equal current density, the ratio of the collected current on the inner and outer collectors is equivalent to the ratio of the current collection areas, expressed as

$$\frac{I_{C1+C2}[\theta,R]}{A_{C1+C2}} = \frac{I_{C1}[\theta,R]}{A_{C1}} \Leftrightarrow \frac{I_{C1+C2}[\theta,R]}{I_{C1}[\theta,R]} = \frac{A_{C1+C2}}{A_{C1}}, \quad (1)$$

where θ is the angular position in the plume in spherical coordinates, R is the downstream measurement radius in spherical coordinates, $I_{C1}[\theta,R]$ is the current to the inner collector as a function of position, $I_{C1+C2}[\theta,R]$ is the combined current to the inner and outer collectors as a function of position, A_{C1} is the cross-sectional collection area of the inner collector, and A_{C1+C2} is the total cross-sectional collection area of the inner and outer collector.

Ratios of ion collection area and ratios of collected current are shown for all background pressures and all distances in Fig. 5. The ratios are calculated based on the collected current or calculated area of configuration 2 (or 4) relative to configuration 1 (or 3). Dashed lines representing the Faraday probe cross-sectional collector area ratios are approximately 15% and 20% greater than the ratios of collected current for the 0.5 and 1.5 mm gap configurations, respectively. Fluctuations in the collected ion current ratio increase beyond $\pm 50^\circ$ from thruster centerline during low background pressure operation. However, ratios of collected ion current are relatively insensitive to variations in distance and pressure in the central core, which indicates that the primary difference between current ratios and area ratios is a systematic error as-

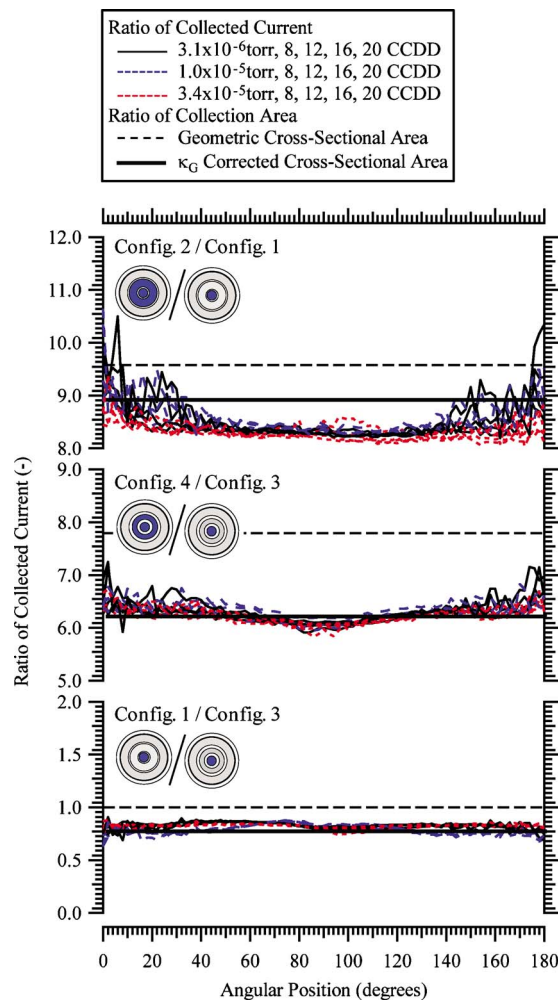


FIG. 5. (Color online) Comparison of collector area ratios and collected current ratios of the 0.5 mm configuration (top), 1.5 mm configuration (middle), and collector 1 (bottom) at 3.1×10^{-6} , 1.0×10^{-5} , and 3.4×10^{-5} torr measured at 8, 12, 16, and 20 CCDD as a function of probe angular position.

sociated with the ion collection area. Variations on the wings are attributed to differences in probe resolution and the orders of magnitude decrease in magnitude of collected current.

Several patterns emerge from the comparison in Fig. 5. The first is that the 1.5 mm gap configuration appears to have a larger systematic error than the 0.5 mm gap configuration. In addition, the ratio of the outer collector area relative to the inner collector area is overpredicted, thereby suggesting that the size of the collector plays a role in this systematic error. The effect of gap width on current to collector 1 is studied as the ratio of configuration 1 relative to configuration 3. While these measurements were performed during different firings of the Hall thruster ion source, the increased gap width corresponds to an increase in the collected current. Identifying and accounting for the systematic error will be the focus of the following section.

IV. DISCUSSION

A. Ion collection in the gap

Current density profiles and ratios of collected current compared to ratios of the probe collection area demonstrated

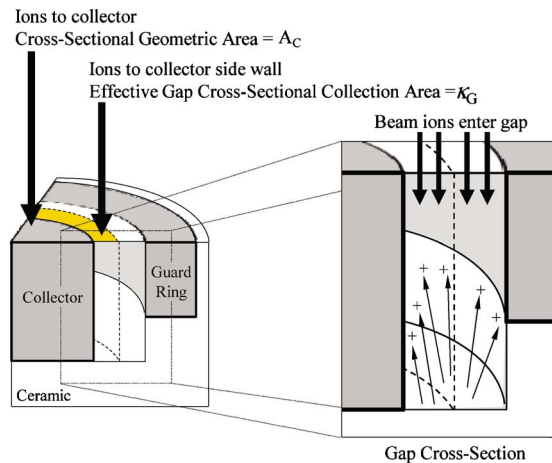


FIG. 6. (Color online) Illustration of ions collected by the sidewalls of the nested Faraday probe and the increase in cross-sectional ion collection area.

that the gap width and probe size have an effect on Faraday probe measurements, and may cause differences in excess of 20%. In addition to the trends observed in Fig. 5, extensive experimental evidence has shown that Faraday probe measurements typically overestimate ion beam current in the Hall thruster plume. This phenomenon is typically attributed to additional ion current from facility effects, but may also be a result of underpredicting the effective ion collection area of the probe. In conventional nude Faraday probe design and analysis, the collection area is calculated as the cross-sectional geometric area of the collector ($A_C = \pi R_C^2$). The gap width is designed to be less than 5–10 Debye lengths to create a flat, uniform sheath over the collector surface.

One possible mechanism for variation from the cross-sectional geometric probe area is the collection of ions within the gap between the collector and guard ring. In this conceptual model, high energy beam ions entering the gap volume impact the ceramic base of the nested Faraday probe, and the resulting low energy ions are collected by the walls of the negatively biased electrodes. A fraction of this current is collected on the sidewalls of the collector, thereby increasing the collected ion current and causing an overestimate of the calculated current density. The effect is shown in Fig. 6, and illustrates the increase in the cross-sectional collection area to account for ion current to the collector sidewall.

To correct for this increase in the effective probe collection area, a Faraday probe gap correction factor κ_G was developed to account for differences in collector geometry and gap width. This correction factor partitions the current collected in the gap volume based on the ratio of the sidewall surface areas.

The geometric probe collection area A_C is increased to account for ions entering the gap volume that are collected by the collector sidewall as

$$A_{\text{effective}} = A_C + \kappa_G, \quad (2)$$

where $A_{\text{effective}}$ is the effective cross-sectional probe collection area. The gap correction factor κ_G is formulated as

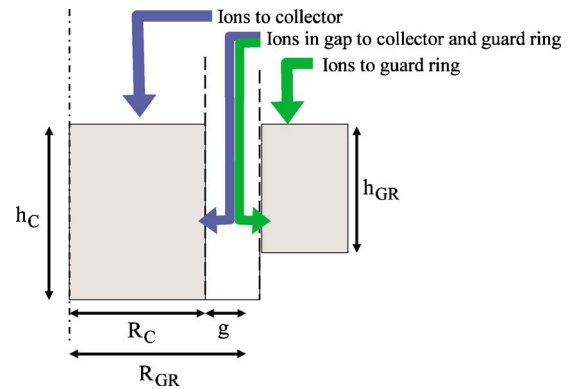


FIG. 7. (Color online) Diagram of the nude Faraday probe collector (outer radius R_C and height h_C), guard ring (inner radius R_{GR} and height h_{GR}), and gap width (g).

$$\begin{aligned} \kappa_G &= A_{\text{gap}} \left(\frac{\bar{A}_C}{\bar{A}_C + \bar{A}_{GR}} \right) \\ &= \pi(R_{GR}^2 - R_C^2) \left(\frac{2\pi R_C h_C}{2\pi R_C h_C + 2\pi R_{GR} h_{GR}} \right), \quad (3) \end{aligned}$$

where A_{gap} is the cross-sectional area of the gap, \bar{A}_C is the sidewall surface area of the collector, and \bar{A}_{GR} is the sidewall surface area of the guard ring. The gap correction is also expressed in terms of probe geometry for the conventional nude Faraday probe with a single collector and guard ring shown in Fig. 7, where R_C is the collector radius, R_{GR} is the guard ring inner radius, g is the gap width, h_C is the height of the collector, and h_{GR} is the height of the guard ring.

Based on this hypothesis, the effective probe collection area would show the greatest increase for designs with a large gap width and a large collector sidewall surface area. The cross-sectional area of a 5–10 Debye length gap width may collect a significant fraction of the measured ion current, especially for a probe with a small collector diameter. It is important to note that the formulation of κ_G in Eq. (3) is only applicable to conventional nude Faraday probes with a ceramic base in the gap volume. The ion collection area of probe designs with a conductive base would be expected to behave differently. This scenario will be studied in greater detail in Sec. IV C.

Corrected and uncorrected collection areas of the four nested Faraday probe configurations are compared in Table II. The gap correction factor increased the cross-sectional areas by approximately 10%–55% to account for ion collection in the gap.

The geometry with smallest collector diameter and the largest gap, configuration 3, had the largest correction in cross-sectional area of approximately 55%. By comparison, the correction to configuration 1 was approximately 17%. This substantial difference highlights the effect of a large gap on a small diameter collector. The gap corrections were larger for the inner collector and larger for the 1.5 mm gap configurations. These trends mirror the patterns established in Figs. 4 and 5.

The corrected area ratios of configuration 2 relative to configuration 1 and configuration 4 relative to configuration

TABLE II. Corrected and uncorrected collection areas of the nested Faraday probe.

	Collection area corrected with κ_G	Uncorrected collection area
0.5 mm gap		
A_{C1} (mm ²)	Configuration 1=34	Configuration 1=29
A_{C1+C2} (mm ²)	Configuration 2=304	Configuration 2=281
A_{C1+C2}/A_{C1}	Area ratio=8.90	Area ratio=9.58
1.5 mm gap		
A_{C1} (mm ²)	Configuration 3=45	Configuration 3=29
A_{C1+C2} (mm ²)	Configuration 4=279	Configuration 4=229
A_{C1+C2}/A_{C1}	Area ratio=6.18	Area ratio=7.80

3 are listed in Table II. These values are compared to the ratio of collected ion current in Fig. 5. The ratios of corrected probe collection area are within 5% of the ratios of collected ion current for all cases. Agreement between the ratios implies that the gap correction factor is accurately partitioning ions in the gap between the collector and guard ring walls for all distances and pressures.

Profiles of ion current density using the corrected probe collection areas are shown in Fig. 8. All four profiles exhibit excellent agreement and the current density of configurations 2, 3, and 4 are indistinguishable throughout the plume. The current density of configuration 1 is larger than the other profiles by a consistent margin. This may be caused by underestimation of the corrected collection area for this configuration, which would also account for the 5% larger corrected area ratio of the 0.5 mm configurations compared to the experimental result in Fig. 5. Possible causes of this deviation include errors in machining tolerance and misalignment. Despite this variation, the uniform current density profiles of four different probe configurations support the

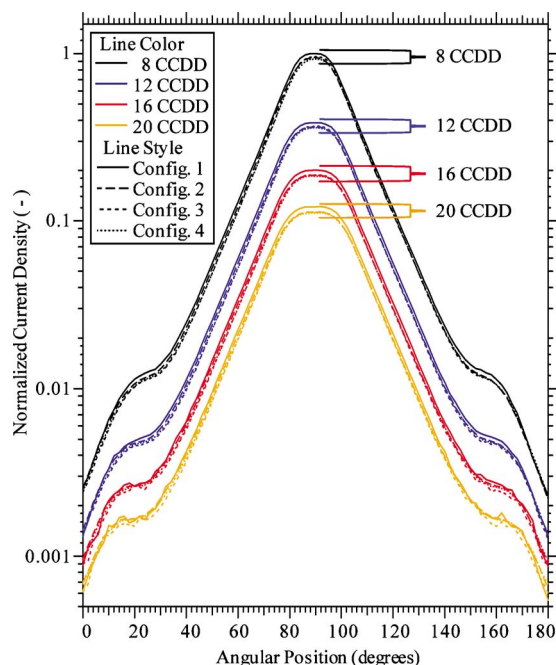


FIG. 8. (Color online) Normalized current density profiles, corrected with κ_G , for configurations 1, 2, 3, and 4 measured at 8, 12, 16, and 20 CCDD with a facility background pressure of 3.1×10^{-6} torr.

assertion that κ_G is accurately accounting for differences in probe geometry based on probe size and gap width.

The uniform current density traces between the 0.5 and 1.5 mm gap configurations in this study indicate fringing field effects above the gap may have a negligible effect on collected current when the gap correction factor is applied, and the 5–10 Debye length gap design criterion may be relaxed. This concept will be studied in the following section by varying the bias potential on the guard ring while holding a constant potential on the collector electrode.

B. Nonuniform bias potential

A nonuniform bias potential across the Faraday probe surface is used to study the current collected in the gap volume and how it is distributed to either the collector or guard ring. The following analysis is idealized and based on the model of ion collection by the sidewalls described in the previous section. With zero bias potential on the guard ring and -15 V on the collector, all current in the gap volume would be measured on the collector. In this case, the effective ion collection area would be the combined cross-sectional area of the collector and gap ($A_C + A_{\text{gap}}$). With a large negative bias potential on the guard ring ($\ll -15$ V) and -15 V on the collector, all current in the gap volume should be collected by the guard ring and the collector will measure less current. In this instance, the effective collection area would simply be the cross-sectional geometric area of the collector (A_C). For uniform current density over the probe collection area, the ratio of collected current at the highest and lowest guard ring bias potential should be equal to the ratio of the collection areas. This formulation is shown in Eq. (4) and is similar to the rationale used in Eq. (1). At a fixed location in the plume, the expression is written as

$$\frac{I_{\text{NFP}}[V_{\text{bias}} = 0]}{A_C + A_{\text{gap}}} = \frac{I_{\text{NFP}}[V_{\text{bias}} = -25]}{A_C} \Leftrightarrow \frac{I_{\text{NFP}}[V_{\text{bias}} = 0]}{I_{\text{NFP}}[V_{\text{bias}} = -25]} = \frac{A_C + A_{\text{gap}}}{A_C}, \quad (4)$$

where V_{bias} is the applied guard ring bias potential and $I_{\text{NFP}}[V_{\text{bias}}]$ is the ion current collected by the nude Faraday probe as a function of guard ring bias potential.

The equivalence in Eq. (4) is examined for the 0.5 mm gap version of the outer collector. Normalized collected current measured with configuration 1 is displayed in Fig. 9 and with configuration 2 is displayed in Fig. 10. For a fixed -15 V on the collector, the collected current as a function of guard ring bias potential is shown from $\theta = 50^\circ$ to $\theta = 130^\circ$ in 10° increments. The examination of configuration 1 in Fig. 9 assesses the inner gap between collector 1 and collector 2, where collector 2 is considered the guard ring. The examination of configuration 2 in Fig. 10 assesses the outer gap between collector 2 and the guard ring, where the collector consists of the combined current from collector 1 and collector 2. These two cases show the variation in collected ion current when the respective guard ring bias voltage is varied from 0 to -25 V. As predicted, the collector current saturates when the guard ring is biased to 0 V. When the guard ring

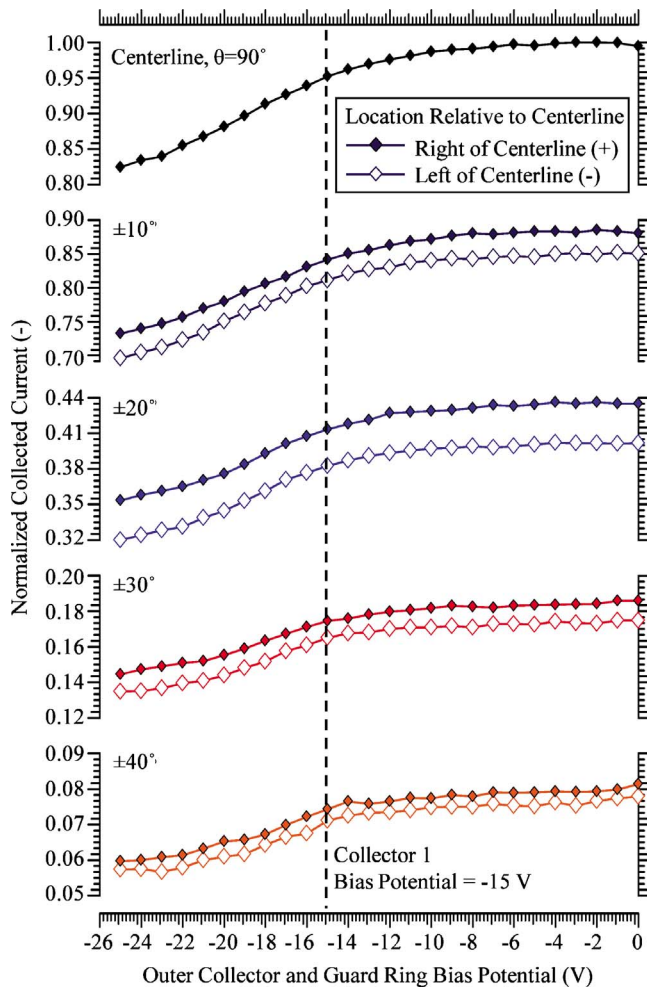


FIG. 9. (Color online) Normalized current to configuration 1 as a function of bias potential on the outer collector and the guard ring. Measurements are normalized to the maximum centerline current for $V_{\text{Bias}}=0$ V, and are shown from $\theta=50^\circ$ to 130° in 10° increments at 20 CCDD with a facility background pressure of 3.1×10^{-6} torr.

bias voltage is decreased, the collector current declines and approaches an asymptote as V_{bias} is further reduced beyond the collector bias voltage of -15 V.

Table III lists the normalized current of configuration 1 and configuration 2 at $V_{\text{bias}}=0$ V and $V_{\text{bias}}=-25$ V on the respective guard rings. In regions of the central core where the collected ion current exhibits a negative slope with -25 V on the guard ring, the asymptotic value is estimated.

The ratio of collected ion currents in Table III may be compared to the ratio of cross-sectional ion collection areas described in Eq. (4) using the dimensions in Table I. In configuration 1, the collector 2 inner diameter relative to the collector 1 outer diameter is approximately $(7.06/2)^2/(6.11/2)^2=1.33$. In configuration 2, the guard ring inner diameter relative to the collector 2 outer diameter is approximately $(20.27/2)^2/(18.91/2)^2=1.15$. In both configurations, the ratio of collected current $I_{\text{NFP}}[0]/I_{\text{NFP}}[-25]$ listed in Table III is approximately equal to the ratio of calculated cross-sectional geometric collection areas. Similar trends were observed for the 1.5 mm gap configurations, but the larger gap distance required a larger negative bias potential on the guard ring to achieve current saturation.

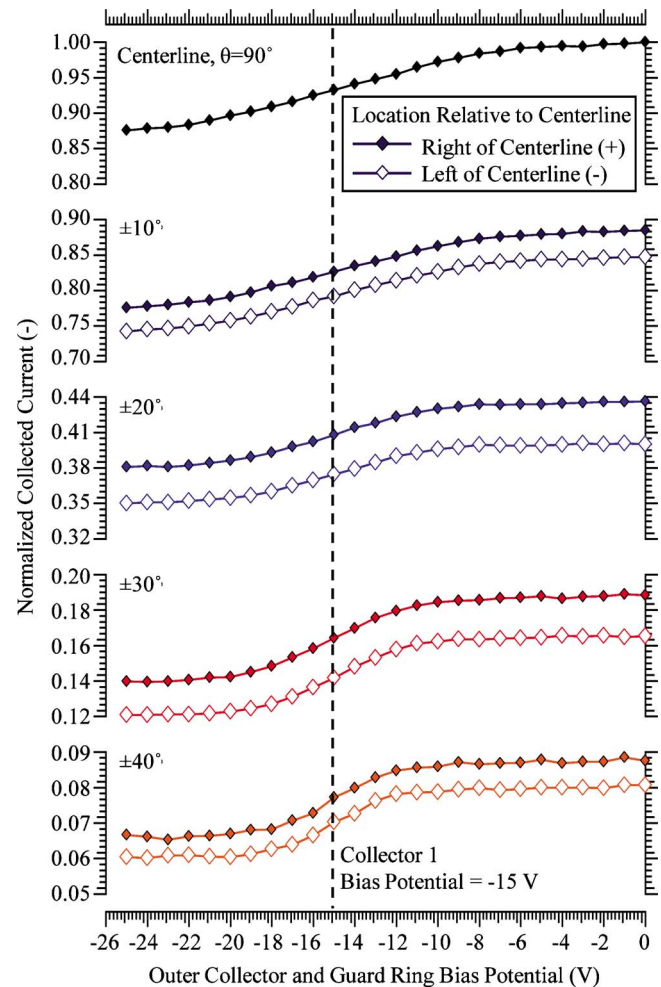


FIG. 10. (Color online) Normalized current to configuration 2 as a function of bias potential on the guard ring. Measurements are normalized to the maximum centerline current for $V_{\text{Bias}}=0$ V, and are shown from $\theta=50^\circ$ to 130° in 10° increments at 20 CCDD with a facility background pressure of 3.1×10^{-6} torr.

These findings indicate that ions in the gap volume were represented by the ratio in Eq. (4), and comprise a non-negligible fraction of the collected current. Thus, conventional nude Faraday probe measurements with equal bias potential on the collector and guard ring necessitate a correction to the cross-sectional collection area. Based on these results and consistent agreement in current density profiles in Fig. 8, it may be possible to relax the probe design criterion of 5–10 Debye lengths if the effective collection area can be determined using probe geometry.

C. Application to past investigation

In a notable investigation of Faraday probe design by Walker *et al.*,^{3,7} measurements of ion current density in a Hall thruster plume with a Jet Propulsion Laboratory (JPL) Faraday probe design were compared to a Glenn Research Center (GRC) nude Faraday probe design. Disparities in the measured current density were attributed to differences in the collector material SEE coefficient (0.15 for steel versus 0.02 for tungsten) and probe geometry. However, a later study conducted at AFRL substituted collectors of differing material while maintaining equivalent Faraday probe geometry.¹²

TABLE III. Normalized collected current when $V_{\text{bias}}=0$ V and $V_{\text{bias}}=-25$ V for the 0.5 mm gap configurations.

Probe position (degrees)	Normalized current, configuration 1 (A)			Normalized current, configuration 2 (A)		
	$V_{\text{bias}}=0$ V	$V_{\text{bias}} \rightarrow$ saturation	$I_{\text{NFP}}[0]$	$V_{\text{bias}}=0$ V	$V_{\text{bias}} \rightarrow$ saturation	$I_{\text{NFP}}[0]$
			$I_{\text{NFP}}[-25]$			$I_{\text{NFP}}[-25]$
50°	0.081	0.06	1.35	0.079	0.068	1.16
60°	0.19	~0.14	1.36	0.18	0.16	1.14
70°	0.43	~0.34	1.26	0.44	0.38	1.14
80°	0.88	~0.71	1.24	0.89	~0.76	1.16
90°	1.0	~0.80	1.25	1.0	~0.86	1.16
100°	0.85	~0.68	1.25	0.85	~0.74	1.14
110°	0.40	~0.31	1.29	0.40	0.34	1.14
120°	0.17	0.13	1.31	0.17	0.15	1.15
130°	0.078	0.058	1.34	0.075	0.065	1.15

These experiments showed negligible difference in the measured ion current density among molybdenum, aluminum, and carbon collectors, and indicated SEE properties had a minimal effect between these materials in the far-field plasma plume. To further evaluate these findings, the gap correction factor is applied to the comparison of Faraday probe design by Walker *et al.*^{3,7} to examine the possibility that differences are due to ion collection in the gap volume. Relevant probe dimensions for the JPL Faraday probe and GRC nude Faraday probe are shown in Table IV. Probe cross sections are displayed in Figs. 11 and 12.

Results from the investigation by Walker *et al.*^{3,7} are listed in Table V for three facility pumping speed configurations of the Large Vacuum Test Facility (LVTF) at the Plasmatronics and Electric Propulsion Laboratory (PEPL) at the University of Michigan. Pumping speeds were 70 000, 140 000, and 250 000 l/s, corresponding to two, four, and seven operational cryopumps. Integrated ion beam current values in Table V are calculated from reported ratios of beam current relative to thruster discharge current: I_{beam}/I_d . The integrated ion beam current is shown in Fig. 13 as a function of pumping speed for all thruster operating conditions tested. The GRC probe measured a larger current density and total ion beam current for all operating conditions. In all cases, the plume profiles were similar in shape, and the authors attributed the disparity in magnitude to collector material SEE properties and an uneven sheath over the GRC probe.³ While both effects may influence the collected current, the effect of ions in the gap volume may be estimated using the gap correction factor described in the previous sections.

In Table IV, the gap correction factor κ_G increases the

ion collection area of the JPL probe by ~5% and the GRC probe by ~14%. However, the guard ring design of the JPL probe differs from the GRC probe and the AFRL nested Faraday probe in that the base of the gap is conductive, and will collect a fraction of the ions in the gap. To account for this difference in the JPL Faraday probe, the surface area of the base was added to the guard ring sidewall surface area in the calculation of κ_G . Ion collection by the area behind the collector of the JPL probe is expected to be minimal and is not accounted for in this rudimentary analysis.

To evaluate the applicability of the gap correction factor to this comparison of Faraday probe designs, the following analysis considers three cases and illustrates the results as the ratio of the total ion beam current of the JPL probe relative to the GRC probe.

- Case 1: No area corrections. Beam current ratio corresponds to the ratio of reported values.
- Case 2: Both areas corrected. Beam currents of both probes are modified according to the gap corrected area values in Table IV.
- Case 3: Only the GRC probe collection area is corrected according to the gap corrected area value in Table IV.

Case 3 evaluates the uncorrected beam current of the JPL probe with the corrected beam current of the GRC probe. Due to the conductive base in the guard ring and internal region of the JPL probe, the gap correction factor may not be suitable as presently formulated. The GRC probe guard ring configuration is a similar design to the AFRL

TABLE IV. Geometry and area correction of the JPL and GRC nude Faraday probes (Ref. 3).

	JPL nude Faraday probe design	GRC nude Faraday probe design
Collector outer diameter (mm)	23.1	19.4
Guard ring inner diameter (mm)	25.4	22.2
Gap width (mm)	1.15	1.40
Cross-sectional collection area (mm ²)	419	296
Cross-sectional area corrected with κ_G (cm ²)	4.40	3.38

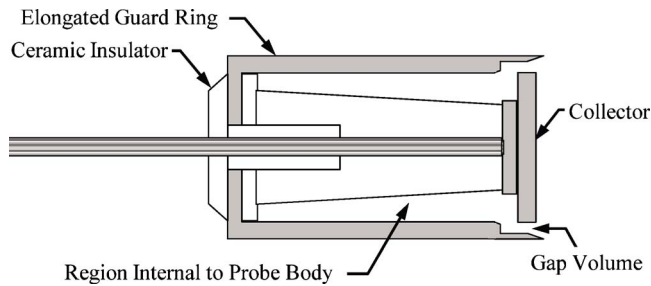


FIG. 11. (Color online) Cross section of the JPL nude Faraday probe.

nested Faraday probe, and the gap correction is more applicable.

The ratios of measured and corrected ion beam current from Table V are illustrated in Fig. 14. For case 1, beam current measured by the JPL probe is $\sim 10\%$ less than the ion beam current measured by the GRC probe. Case 2 shows the effect of correcting both probe collection areas for the gap width, and resulted in good agreement to within 3% for all thruster operating conditions at the high background pressures, corresponding to facility pumping speeds of 70 000 and 140 000 l/s. The correction appears to be more applicable in the highest background pressure case. In case 3, the GRC probe and JPL probe beam currents exhibited very good agreement for all thruster operating conditions at the lowest facility background pressure, corresponding to a facility pumping speed of 250 000 l/s.

As the number of pumps was decreased, and hence the facility background pressure and charge-exchange (CEX) ion number density in the plume increased, the ratios of the integrated beam current increased for all cases. This phenomenon may be explained based on the distribution of ions to the guard ring and collector sidewalls within the JPL probe gap volume. At low background pressure, incoming ions entering gap are primarily collected by the conductive base in the guard ring, and the ion collection area is approximately equal to the cross-sectional probe collection area A_c . Therefore no correction is necessary. At elevated facility background pressure with increased low-energy CEX ions, a significant fraction of the ions entering the gap volume are

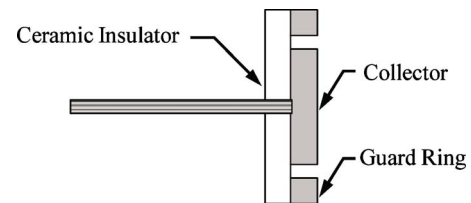


FIG. 12. (Color online) Cross section of the GRC nude Faraday probe.

collected by the collector sidewall. This increases the measured ion current and necessitates evaluation of the effective cross-sectional collection area of the probe, as illustrated in Fig. 15. In this hypothesis, the partition of ions in the gap volume of the JPL probe is a function of background pressure and is not adequately described by the gap correction factor, κ_G . Therefore, the cross-sectional area of the JPL nude Faraday probe would be appropriate at low background pressure, but additional characterization may be required to determine the collection area at high facility background pressure. In contrast, the correction κ_G is expected to be applicable for the GRC nude Faraday probe regardless of facility background pressure, since it has a ceramic base.

Applying the gap correction factor to the investigation by Walker revealed differences associated with Faraday probe design and the importance of accurately assessing ion collection characteristics in the gap. If the effective ion collection area of the JPL probe varies with background pressure, characterization of facility effects with measurement distance and pressure using the JPL probe may introduce unknown trends. Although the JPL Faraday probe may not require an area correction at low facility background pressures, the collection areas of the conventional GRC Faraday probe and the AFRL nested Faraday probe designs are less difficult to characterize and therefore are more suitable for investigations of beam divergence and facility effects when the Debye length and CEX ion number density varies throughout the plume.

V. SUMMARY AND CONCLUSIONS

A nested Faraday probe with two concentric collectors and an outer guard ring was designed and fabricated at

TABLE V. Comparison of the JPL and GRC Faraday probes for variations in background pressure and thruster operation, from Walker *et al.* (Ref. 7).

Number of LVTF cryopumps	Background pressure (torr)	Discharge voltage (V)	Discharge current (V)	Reported ion beam current (A)		Gap corrected ion beam current (A)	
				JPL probe	GRC probe	JPL probe	GRC probe
2	1.3×10^{-5}	300	4.39	3.78	4.13	3.59	3.61
4	7.6×10^{-6}	300	4.37	3.89	4.24	3.70	3.71
7	4.3×10^{-6}	300	4.35	3.92	4.44	3.73	3.88
2	2.3×10^{-5}	300	10.23	9.10	9.92	8.66	8.68
4	1.3×10^{-5}	300	10.14	9.13	10.04	8.68	8.78
7	7.7×10^{-6}	300	10.22	9.20	10.42	8.75	9.11
2	1.3×10^{-5}	500	5.01	4.16	4.51	3.96	3.94
4	7.6×10^{-6}	500	4.93	4.24	4.73	4.03	4.14
7	4.6×10^{-6}	500	4.89	4.40	5.04	4.19	4.40
2	2.3×10^{-5}	500	10.62	9.77	10.62	9.30	9.29
4	1.3×10^{-5}	500	10.66	10.02	11.09	9.53	9.69
7	7.7×10^{-6}	500	10.72	9.86	11.26	9.38	9.84

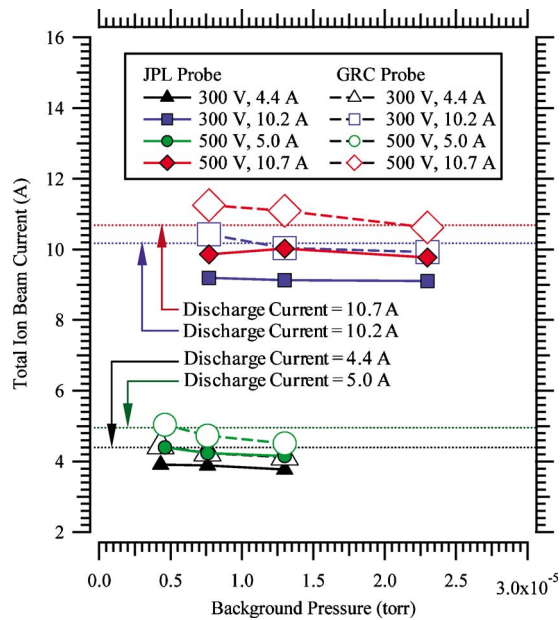


FIG. 13. (Color online) Total ion beam current of the NASA173M-v1 as a function of background pressure for the JPL and GRC nude Faraday probes from Walker *et al.* (Ref. 3).

AFRL to investigate the effects of collector geometry on Faraday probe ion collection characteristics. The probe was characterized over a range of background pressures and downstream distances to isolate effects specific to probe geometry. Ion current collection by the sidewall of the collector was identified as a source of systematic error in conventional Faraday probe data analysis, and results in artificially elevated current density profiles when the cross-sectional collector area is used in calculations. A correction factor was proposed to adjust the effective probe collection area for ions collected by the walls in the gap volume.

To further illustrate the nature of the gap correction factor, a dissimilar bias potential was applied to the collector and guard ring of the nested probe. Depending on the potential difference between the guard ring and collector, this study demonstrated the ability to collect nearly all of the ions in the gap volume on the sidewall of the guard ring or the sidewall of the collector. Correct application of the correction factors to both the 0.5 and the 1.5 mm gap configurations resulted in equivalent plume profiles despite the 1.5 mm gap being approximately 15–30 Debye lengths. Although the 1.5 mm gap configuration may introduce a non-uniform sheath over the Faraday probe collecting surface, the nonuniformity is primarily over the gap width and appears to be accounted for by distributing the ions in the gap volume using the gap correction factor. These results indicate that the conventional design criteria of 5–10 Debye lengths may be relaxed using the proposed analytical technique. This result has important implications for Faraday probes designed to operate over a range of plasma properties with widely varying Debye length.

The analytical techniques were applied to a past investigation that compared two Faraday probe designs, and led to new insight for differences associated with probe geometry. A hypothesis was proposed for ion collection in Faraday

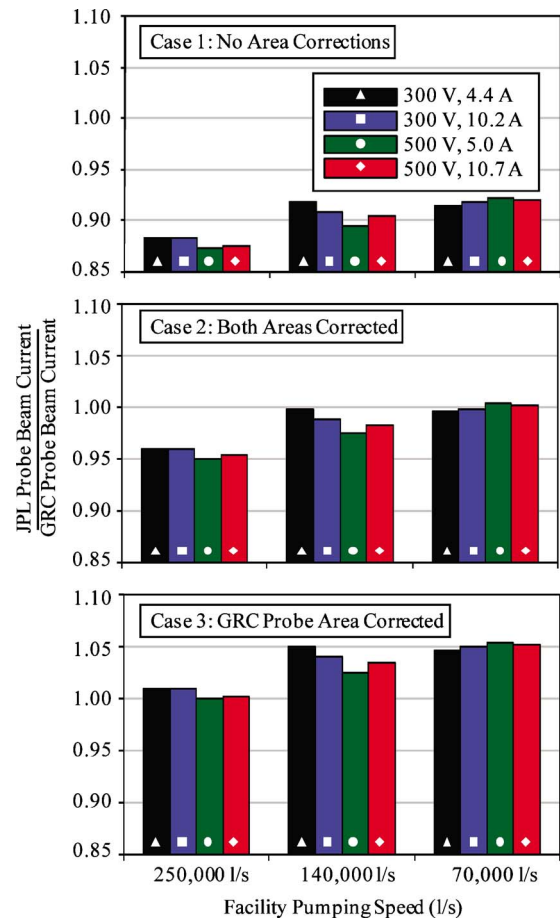


FIG. 14. (Color online) Ratio of total ion beam current of the JPL nude Faraday probe relative to the GRC nude Faraday probe with variations in facility pumping speed for the case 1 (top), case 2 (middle), and case 3 (bottom).

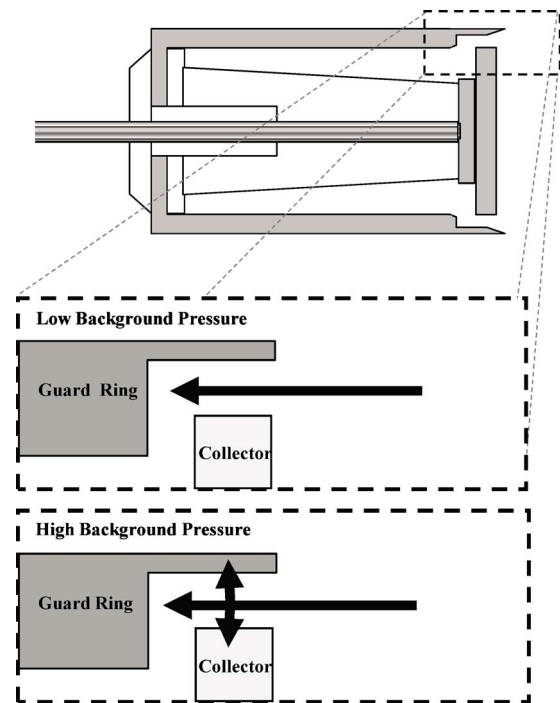


FIG. 15. (Color online) Illustration of ion collection in the gap volume of the JPL Faraday probe for high and low facility background pressure.

probes with a conductive surface at the base of the gap volume. Facility background pressure is believed to effect probes of this design, and will likely complicate characterization of electric propulsion plumes. In contrast, the gap correction factor demonstrated consistent agreement in plume profiles by the nested Faraday probe over a wide range of measurement distance and background pressure. Therefore, nude Faraday probes with a ceramic base are more suitable for characterization of facility effects and studies of a plasma plume with a range of Debye lengths.

ACKNOWLEDGMENTS

The authors would like to thank Dr. Justin Koo and the late Dr. Bill Larson for numerous insightful discussions, and Mr. Mike Nakles and Mr. Garrett Reed for assistance with the experimental setup and data acquisition.

¹M. L. R. Walker, A. L. Victor, R. R. Hofer, and A. D. Gallimore, *J. Propul. Power* **21**, 408 (2005).

²D. H. Manzella and J. M. Sankovic, "Hall Thruster Ion Beam Characterization," AIAA-95-2927, Presented at the 31st AIAA Joint Propulsion Conference, San Diego, CA, 10–12 July, 1995 .

³M. L. R. Walker, R. R. Hofer, and A. D. Gallimore, *J. Propul. Power* **22**, 205 (2006).

⁴J. L. Rovey, M. L. R. Walker, A. D. Gallimore, and P. Y. Peterson, *Rev. Sci. Instrum.* **77**, 013503 (2006).

⁵K. H. de Grys, D. L. Tilley, and R. S. Aadland, "BPT Hall Thruster Plume Characteristics," AIAA-99-2283, Presented at the 35th AIAA Joint Propulsion Conference, Los Angeles, CA, 20–24 June, 1999.

⁶R. R. Hofer, M. L. R. Walker, and A. D. Gallimore, "A Comparison of Nude and Collimated Faraday Probes for Use with Hall Thrusters," IEPC-01-020, Presented at the 27th International Electric Propulsion Conference, Pasadena, CA, 15–19 October, 2001.

⁷M. L. R. Walker, R. R. Hofer, and A. D. Gallimore, "The Effects of Nude Faraday Probe Design and Vacuum Facility Backpressure on the Measured Ion Current Density Profile of Hall Thruster Plumes," AIAA-2002-4253, Presented at the 38th AIAA Joint Propulsion Conference, Indianapolis, IN, 7–10 July, 2002.

⁸J. S. Pearlman, *Rev. Sci. Instrum.* **48**, 1064 (1977).

⁹G. Gerdin, W. Stygar, and F. Venneri, *J. Appl. Phys.* **52**, 3269 (1981).

¹⁰W. H. Bostick, H. Kilic, V. Nardi, and C. W. Powell, *Nucl. Fusion* **33**, 413 (1993).

¹¹T. A. Shelkovenko, S. A. Pikuz, I. C. Blesener, R. D. McBride, K. S. Bell, D. A. Hammer, A. V. Agafonov, V. M. Romanova, and A. R. Mingaleev, *Rev. Sci. Instrum.* **79**, 10E316 (2008).

¹²S. F. Engelman and J. M. Fife, "Hemispherical Measurements of the SPT-140 Plume," AIAA-2002-4255, Presented at the 38th AIAA Joint Propulsion Conference, Indianapolis, IN, 7–10 July, 2002.

¹³M. R. Nakles and W. A. Hargus, Jr. (personal communication).